
2 Magnetic Resonance: Applications in Dementia

2.1 Magnetic Resonance Techniques (Figs. 2.1-1 to 2.1-14)

Since MR techniques have become available sensitivity and, to a lesser extent, specificity in the diagnosis of dementias has enormously increased. It is, however, important to use the proper techniques to extract the maximum information from the images and to answer specific questions. The advantages and disadvantages of specific techniques must be known, to minimize the risk of missing a diagnosis or reporting incompletely. The available arsenal of techniques in MRI is impressive and it is rarely possible to perform all possible MR techniques in one session in one patient, if that were desirable.

2.1.1 Overview of Available MR Techniques

2.1.1.1 *Conventional T1- and T2-Weighted Spin Echo (SE) Techniques*

The main feature of conventional T1- and T2-weighted SE techniques is refocusing of the transverse magnetization after excitation by a 180° radio-frequency (RF) pulse. SE sequences are the workhorses of MR studies and still have value in many cases. T1-weighted SE sequences give anatomical detail with a high contrast between white and gray matter; pathology is less well delineated. T1-weighted SE images are also used when T1-prevalent contrast media are used. These contrast media shorten the T1 relaxation time, leading to a higher

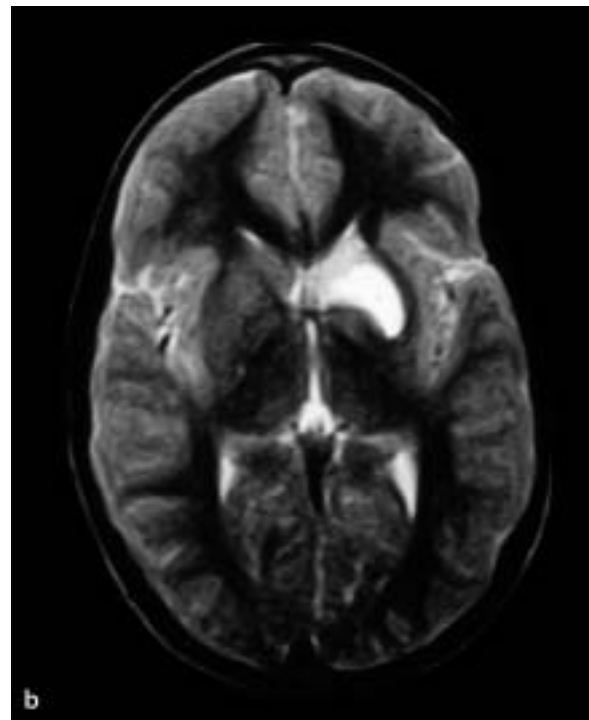
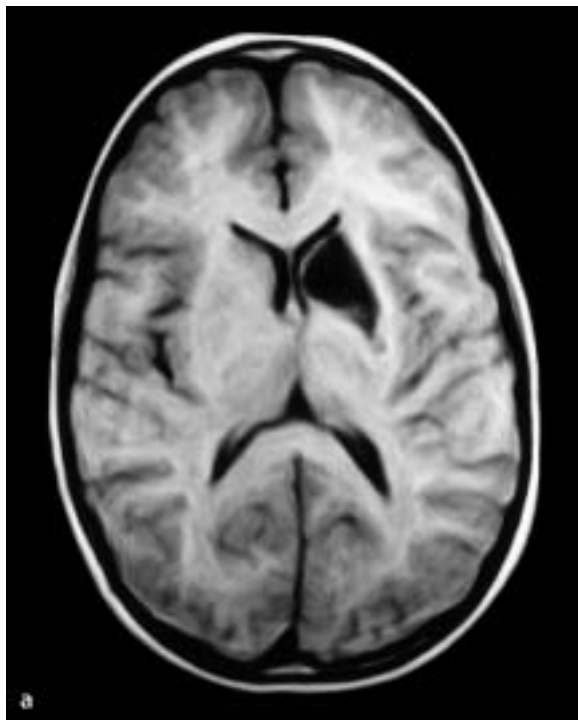


Fig. 2.1-1 a, b. Transverse spin echo (SE) images, respectively T1-weighted (a) and T2-weighted (b). T1-weighted images show cerebrospinal fluid (CSF) black and give anatomical detail. The lesion in the left caudate region in this image is hypointense and well defined. On the conventional T2-weighted image CSF is bright as is the lesion on the left side. In the central nervous system pathological tissue often

is hypo- or isointense on T1-weighted images and hyperintense on T2-weighted images. It is not possible on these two images to conclude whether the lesion is cystic or solid. Therefore one needs to add other sequences. In this case the lesion is solid: a 17-year-old boy with Sydenham's chorea. This one-sided caudate lesion is highly characteristic for the disease

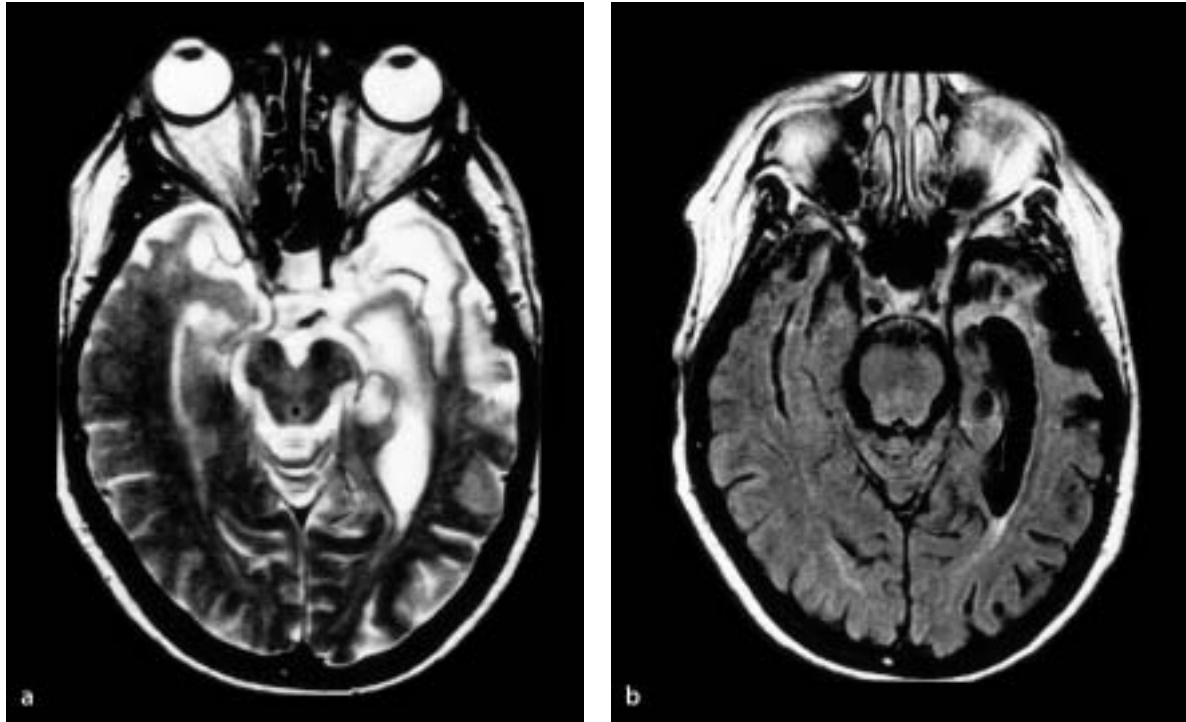


Fig. 2.1-2 a, b. Transverse turbo (fast) SE T2-weighted image (a) through the level of the mesencephalon and at about the same level a FLAIR (dark fluid) image (b) in a patient with an asymmetrical cortical degenerative syndrome. Both images show the predominant left temporal lobe degeneration, with widening of the temporal horn, loss of structure

in the hippocampus, signal changes in the white matter of both temporal lobes on both sides, worse on the left, and irregular cortical atrophy, also more conspicuous on the left side. The FLAIR image highlights the gliotic part of the white matter changes in the temporal pole

signal where the blood-brain barrier is disturbed. Conventional T2-weighted sequences provide less contrast between gray and white matter, but excellent contrast between normal brain tissue and pathology, as well as with cerebrospinal fluid (CSF) (Fig. 2.1-1).

2.1.1.2 Turbo or Fast Spin Echo Sequences (TSE)

In conventional SE sequences, each RF excitation pulse is followed by a single phase encoding step. In TSE sequences each RF excitation pulse is followed by multiple (typically between 3 and 25) phase encoding steps, saving a considerable amount of time. The repetitive 180° pulses reduce the susceptibility to magnetic field inhomogeneities. Also, because of the difference between echo time in conventional SE and the so-called effective echo time in TSE (the echo in the middle of k-space) fat will not have lost signal at long echo times. Both factors have to be taken into account when reading the images. As a result of increased incidental magnetization transfer effects, brain tissue will be darker, and CSF relatively brighter (Fig. 2.1-2a).

2.1.1.3 Fluid Attenuation Inversion Recovery (FLAIR)

FLAIR is a strongly T2-weighted variant of an inversion recovery sequence, with the inversion time chosen to nullify the signal of water. The advantage of this sequence is that lesions around the ventricles are easily seen. The contrast between gray and white matter is low (especially in the elderly population), facilitating detection of lesions in the cortical and subcortical region. The method has gained acclaim in many centers and its use is standard, certainly in combination with a TSE T2-weighted sequence. FLAIR performs less well than SE techniques in the posterior fossa; also its use in the spinal cord so far has been disappointing. Another disadvantage of FLAIR is the suppression of pathology with extremely prolonged T1 relaxation time (comparable to free water), and the inability to separate structures with low signal (such as vessels, calcifications) from CSF (Fig. 2.1-2b).

2.1.1.4 Gradient Echo (GE) Sequences

Instead of using a 180° RF pulse, an echo can also be produced by reversal of gradients, which again saves time. Since no refocusing pulse is used, the inhomogeneities in the magnetic field will not be cancelled, introducing susceptibility to local disturbances of the magnetic field. While this leads to artifacts at bone and air interfaces, this feature can also be used to advantage to detect calcifications and blood pigments. Also in this sequence a turbo factor can be used: multiple phase encoding increments with one excitation. The ultimate sequence is the single-shot echo-planar sequence, where all phase encoding steps are taken with one RF excitation (Fig. 2.1-3, p. 8).

Additional Techniques

There are several techniques that can be added to the abovementioned “carrier” sequences, of which two are mentioned here: magnetization transfer and fat suppression. Both techniques have a distinct influence on the image formation.

Magnetization Transfer Imaging (MTI) is based upon the difference between “bound” and “free” water protons. Bound water is part of macromolecular structures with a broad range of resonance frequencies, whereas free water protons have a smaller resonance frequency range (a smaller peak in spectral plots). By using a special off-resonance pulse it is possible to presaturate these bound protons, in which condition magnetization will be transferred from the free protons to the bound protons, leading to a lowering of the MR signal. The integrity of the examined tissue is directly related to the measure of bound protons. MTI and the magnetization transfer ratio (MTR; obtained by dividing the signal intensities in the region of interest without a magnetization transfer prepulse by those with such a prepulse and multiplying by 100) are considered to be an expression of tissue integrity.

Fat Suppression can be achieved by different means. Because of the short T2 relaxation time of fat, it will have no signal in sequences that express long T2 relaxation times, and therefore in sequences with long echo times (with the exception of fast spin echo techniques: see Sect. 2.1.1.2). A different technique uses the small difference in resonance frequency between protons in fat and protons in water. By applying a prepulse with the exact resonance frequency of fat protons, their signal can be annihilated. In particular neurological, oncological and endocrinological problems these fat suppression techniques are very important.

The following four techniques are even less routinely employed in clinical practice and will be discussed in more detail below:

- ▶ MR diffusion weighted imaging (DWI)
- ▶ MR perfusion imaging (PI)
- ▶ MR spectroscopy (MRS)
- ▶ MR neurofunctional imaging

2.1.1.5 Diffusion Weighted Magnetic Resonance Imaging (DWI)

Diffusion weighted MRI (DWI) uses water movement and transport of water in biological tissues as a source of contrast. Therefore DWI can be used to obtain information about molecular displacement over distances comparable to the cell's dimensions, and, consequently, about geometry and spatial organization of tissue compartments. One can also gather functional insight concerning exchanges between these compartments in various normal or disease states. In the presence of magnetic field gradients, protons carried by free moving water molecules undergo a phase shift of their transverse magnetization. Normal diffusion is characterized by the random Brownian displacements of molecules, resulting in phase shifts that are widely dispersed. The phase dispersion results in attenuation of the MR signal. The amount of attenuation depends directly on the amplitude of the molecular displacement and the intensity of the magnetic field gradient. In conventional MRI diffusion effects are extremely small and negligible. By adding a strong magnetic field gradient to an (arbitrary) imaging pulse sequence, diffusion sensitivity becomes stronger and measurable. Strength and deviation of the gradient pulse determine the degree of diffusion weighting: the “diffusion sensitivity” or “b-value”.

On DWI, structures with unlimited diffusion (such as CSF) are dark, while structures with restricted diffusion are bright. In the human brain gray matter diffusion is isotropic. White matter diffusion is extremely variable and dependent on the relative orientation of the myelin sheaths along the axonal tracts. The myelin sheaths partially restrict free diffusion: this restriction of molecular motions results in anisotropic diffusion. This can be used to advantage. By applying the diffusion gradient in one direction the pulse sequence is sensitized for diffusion in that direction. Fiber tracts parallel to this gradient will show maximal signal loss, whereas the effect is minimal if the gradient is perpendicular to the fiber tracts. By applying gradients in three or more directions one can choose to display the ani-

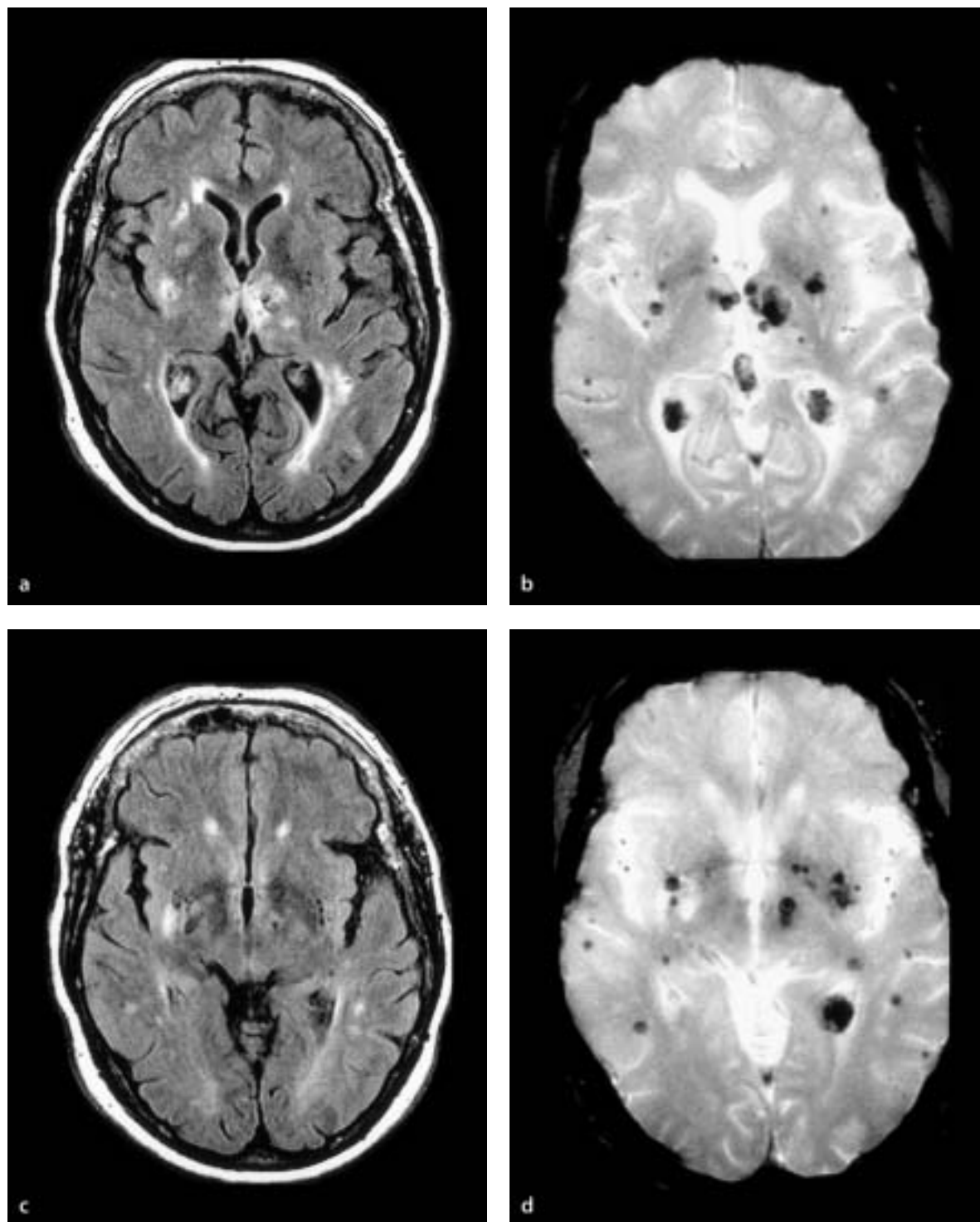


Fig. 2.1-3. **a, c** Two transverse FLAIR images in a 54-year-old woman who was treated for breast carcinoma 6 years previously. She had received postoperative radiation and chemotherapy and lately complained of headaches and dizziness. The FLAIR images show multiple hyperintense abnormalities, mostly located in the basal ganglia, thalamus

and around the ventricles. **b, d** The corresponding T2*-weighted GE images reveal multiple rounded hypointense lesions of different size spreading much further outward; these are probably hemorrhagic-necrotic metastases. The added value of the gradient-echo images is clear

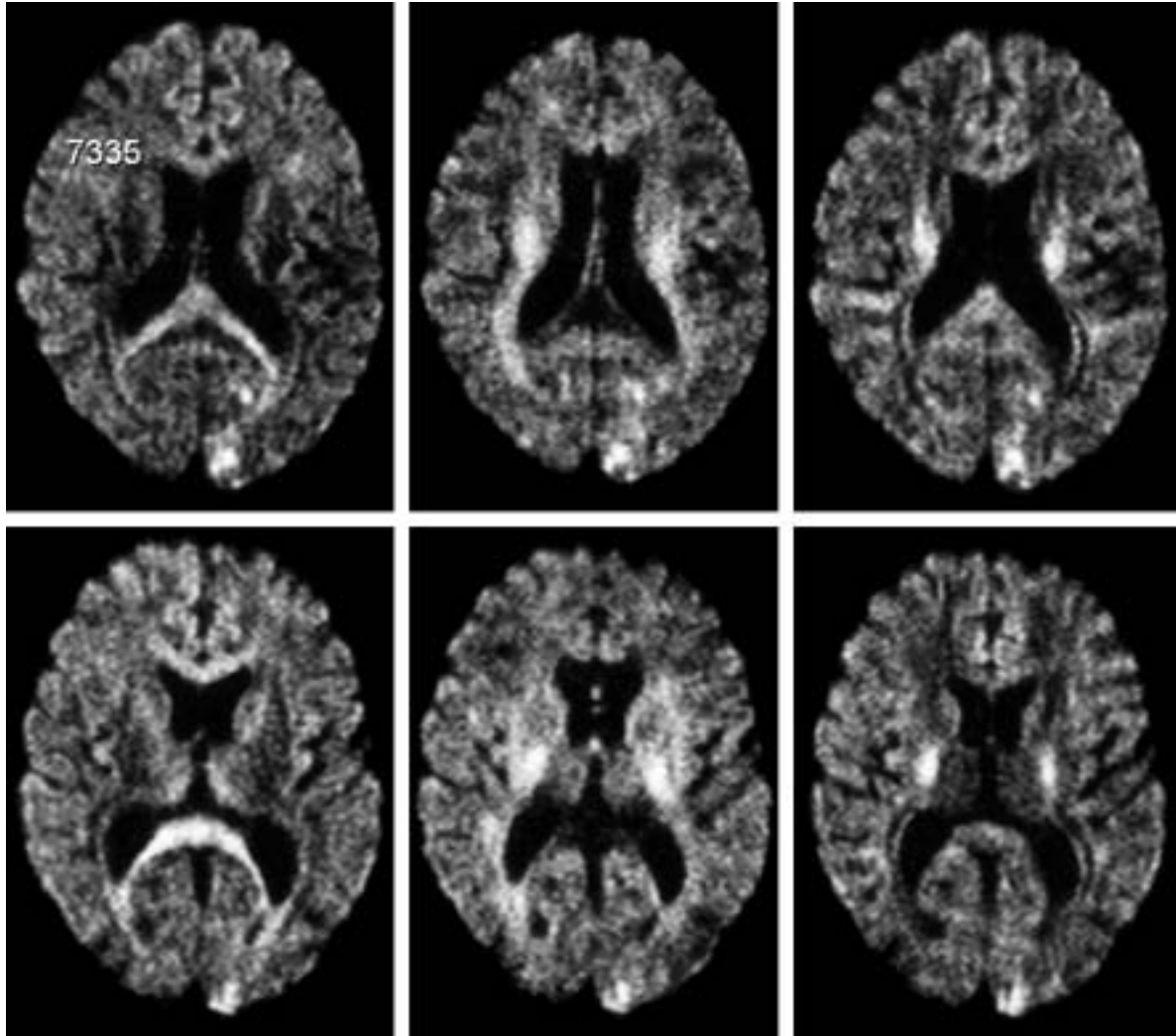


Fig. 2.1-4. Anisotropic diffusion images at two different levels. In the first column the diffusion sensitized gradient is perpendicular to the image plane (z -axis); in the second column, from left to right (x -axis= read direction); in the third column, in the lower-upper direction, y -axis or phase encoding direction. The white matter tracts have the highest

signal intensity when the gradient direction is perpendicular to the long axis of the fiber tract. In this patient with an acute left-sided hemianopsia the only constant lesion with hyperintensity is in the left occipital pole, representing an infarction

sotropy of the white matter in studying, for example, myelination progress; to use the values of diffusion in different directions and average the values to cancel the anisotropy and obtain so-called trace maps, for example for the diagnosis of infarctions and infections; or to maximize the anisotropy information by using multiple gradients, six or more in different directions, to obtain diffusion tensor measurements, which allow the display of fiber tracts in the brain. Interruption of myelin sheaths by demyelination, cytotoxic edema in infarction, inflammation or infection will be shown with high sensitivity by DWI. The superiority of DWI to conventional MRI in the detection of recent infarctions has been demonstrated

in numerous studies. Other pathologies, such as vacuolating myelinopathy and spongiform encephalopathies, can also be studied with this technique.

Summarizing the ways to analyze, display and calculate DWI we can distinguish:

- (A) Anisotropic diffusion. The effects of applying a diffusion gradient in slice, phase and read direction are measured. On the images white matter tracts will show a high signal when the gradient is perpendicular to the long axis of the fiber tract. This technique has advantages in disorders in which fiber tracks are disrupted, for example in multiple sclerosis, or for assessing the progress of myelination (Fig. 2.1-4).

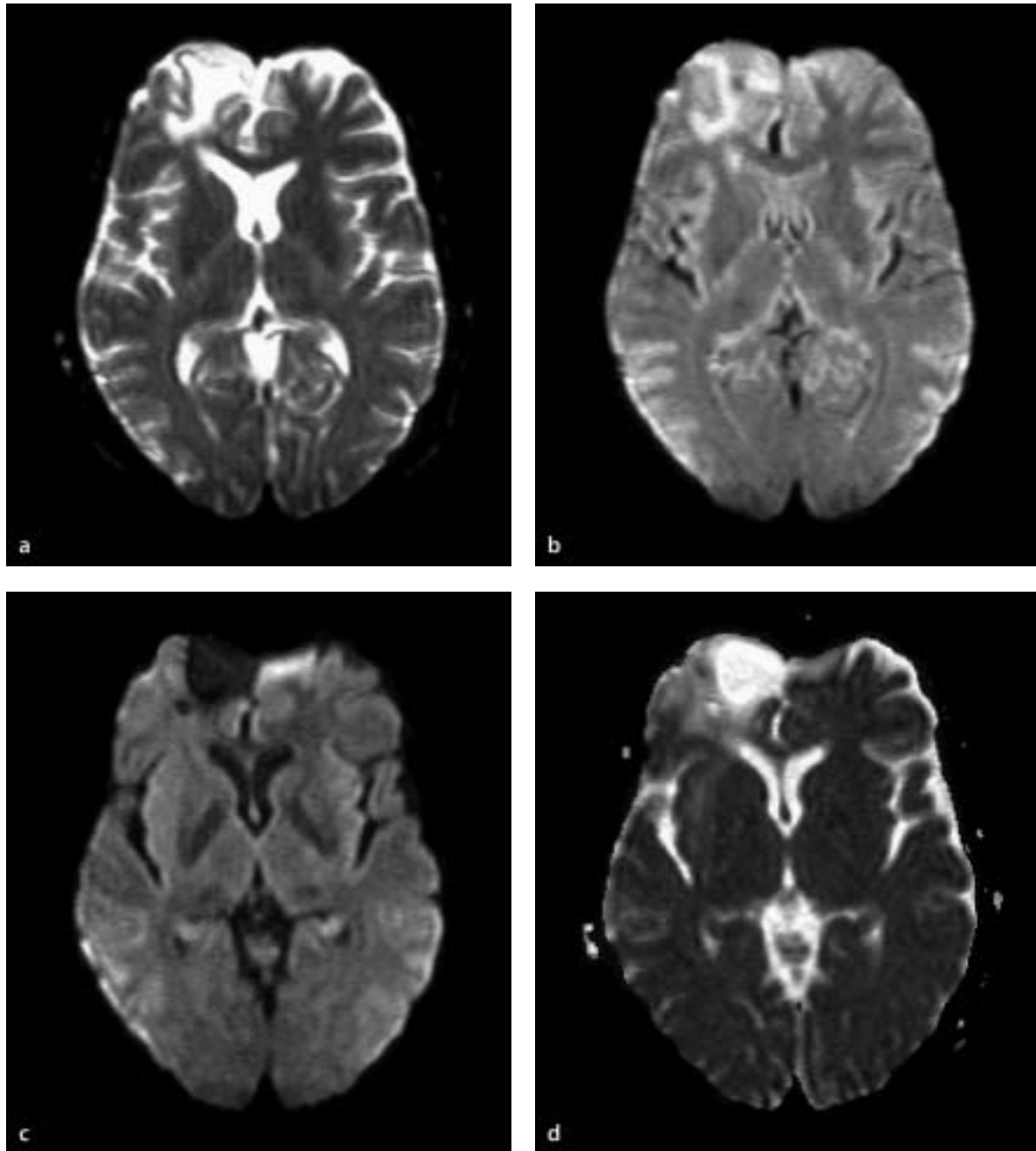


Fig. 2.1-5 a–d. A series of images is presented. **a** An echo-planar image, T2*-weighted, shows a small cyst in the right frontal pole. **b, c** The effect of applying diffusion gradients of a diffusion sensitivity of respectively 500 and 1000 mm^2/s . Note that at a sensitivity of 500 the cyst appears bright, somewhat brighter than the CSF. At a sensitivity of

1000 the cyst contents follow the signal intensity of the CSF. **d** From diffusion measurements at different b levels an Apparent Diffusion Coefficients (ADC) map can be constructed. This makes clear that the cyst contains CSF-like fluid and has a high diffusion coefficient

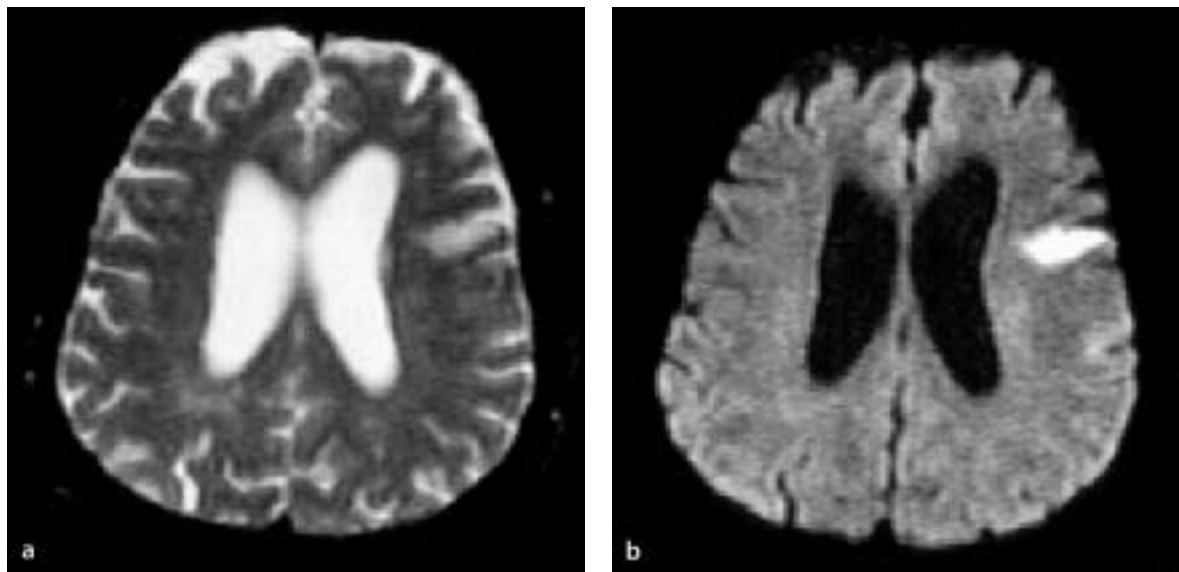


Fig. 2.1-6 a, b. Diffusion weighted imaging has been of great importance in identifying recent infarctions. It plays an important role in the early diagnosis of cerebral infarctions in stroke units. These images were obtained at the same level,

one without diffusion gradient (**a**), the other with a diffusion sensitivity of $b=1000 \text{ mm}^2/\text{s}$ (**b**). **a** shows a rather non-specific lesion in the frontal operculum; **b** the DWI makes clear that the lesion is a recent infarction

- (B) Diffusion trace maps can be calculated, by averaging the effects of gradients in three or more directions, and displaying the results of the averaged measurements. According to Bassler et al. (2000) anisotropic diffusion can be represented by a symmetrical 3×3 diffusion tensor, D , at each position in space and can be modeled as ellipsoidal water movements for modeling of MRI data. Anisotropic movement effects can thus be removed from the image by creating a directionally averaged diffusivity: a trace map (Fig. 2.1-5a-c).
- (C) Diffusion coefficients can be calculated from acquisitions with different diffusion weighting (or b -values). The apparent diffusion coefficient (ADC) can be estimated from the slope of the diffusion measurements with higher b -values and also displayed as images. The term "apparent" is used because the diffusion coefficient is calculated from the mean values of a given voxel, in tissue in which restriction of diffusion is not identical for all components, while diffusion is manipulated by gradient switching (Figs. 2.1-5d, 2.1-6).
- (D) Tensor diffusion weighting is achieved by using measurements in at least seven different gradient directions, for example a combination of orthogonal and tetrahedral gradient directions, or using a polyhedral concept to direct the gradients. By this technique intensity and direction

of the local diffusion can be obtained. All other measurements can be calculated from these data, such as fractional anisotropy (the amount of anisotropy present in a voxel), ADC values, etc. With appropriate software programs it is possible to perform fiber tracking, demonstrating in detail the anatomy of the white matter tracts (Fig. 2.1-7).

DWI in dementia can be very helpful in patients with suspicion of a vascular dementia, to identify cytotoxic edema as an indication of recent infarction or ischemia, or to separate older from newer lesions. Especially in cytotoxic edema diffusion is strongly limited in both the extracellular and intracellular compartments and the involved areas will have high signal on the DWI images. Conversely, the ADC values in such areas will be lowered. In vacuolating myelinopathy and spongiform encephalopathies, characterized histologically by the formation of a multitude of small vacuoles in the tissue, diffusion movements are restricted even more than in cytotoxic edema. In white matter disorders with vacuolating myelinopathy (e.g. Kearns-Sayre disease, L-dihydroxyglutaric aciduria, maple syrup urine disease, and many other organic acidurias) the affected white matter shows a high signal on DWI. In cases with cortical involvement, for example in (transmissible) spongiform encephalopathies, DWI may show the cortical involvement when other tech-

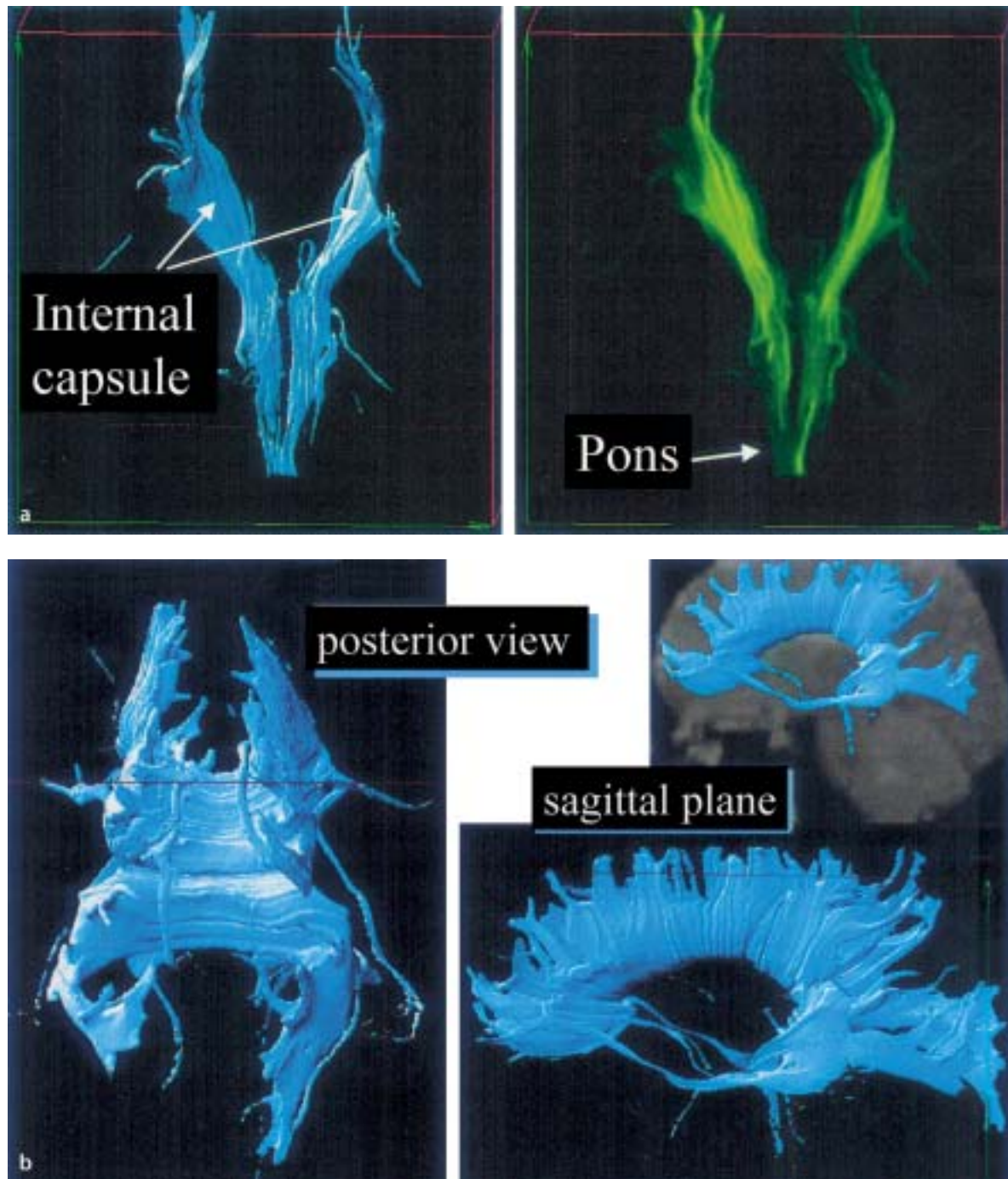


Fig. 2.1-7 a, b. Diffusion tensor measurements create the possibility of fiber tracking, as beautifully demonstrated here by Peter Basser's group. We show two examples, one illustrating the reconstruction of the corticospinal tracts (a), the other different perspectives of the reconstructed fi-

bers of the corpus callosum (b). This possibility creates new ways of research, in neonates, children and adults, in diseases interfering with white matter tracts. (From Basser et al. 2000, with permission)

niques fail to do so. For research purposes fiber tracking, when sufficiently refined, will probably have a great impact on our understanding of the pathophysiology of dementia (Basser et al. 2000).

2.1.1.6 MR Perfusion Imaging

In MR perfusion imaging of the brain, the passage of a bolus of contrast agent through the brain parenchyma is imaged by dynamic T2*-weighted MRI (Fig. 2.1-8, p. 14). Information from the first passage of the contrast material through the regional microcirculation is obtained from changes in the resulting MR signal. For perfusion weighted MRI, a bolus injection of a gadolinium-containing contrast medium is used, usually at a slightly higher dose than normally used. The effect of the paramagnetic agents followed using a T2*-weighted technique, typically an EPI sequence. During the injection of the bolus, multislice EPI images are made through the brain, typically with 1–2 s intervals, and the changes in signal intensity per voxel are measured and displayed. Estimation of relative cerebral blood flow (rCBF), time-to-peak (TTP) and mean transit time (MTT) can be performed and displayed.

The kind of information that can be obtained with MR perfusion imaging is similar to that from positron emission tomography (PET), although the absolute quantitation of the measurements on MR is even more difficult. On the other hand the spatial resolution of MR is higher. The combination of perfusion and diffusion imaging on MR is very helpful in the estimation of a match or mismatch of the findings on perfusion and diffusion. This is, for example, helpful in the estimation of the time window for therapy in acute strokes.

Perfusion weighting in patients with dementia can be helpful in, for example, Alzheimer's disease, where a temporo-parietal hypoperfusion can be found, and in frontotemporal dementias (symmetrical or asymmetrical), where a fronto-temporal hypoperfusion can be found, even in early stages of the disease.

2.1.1.7 MR Spectroscopy

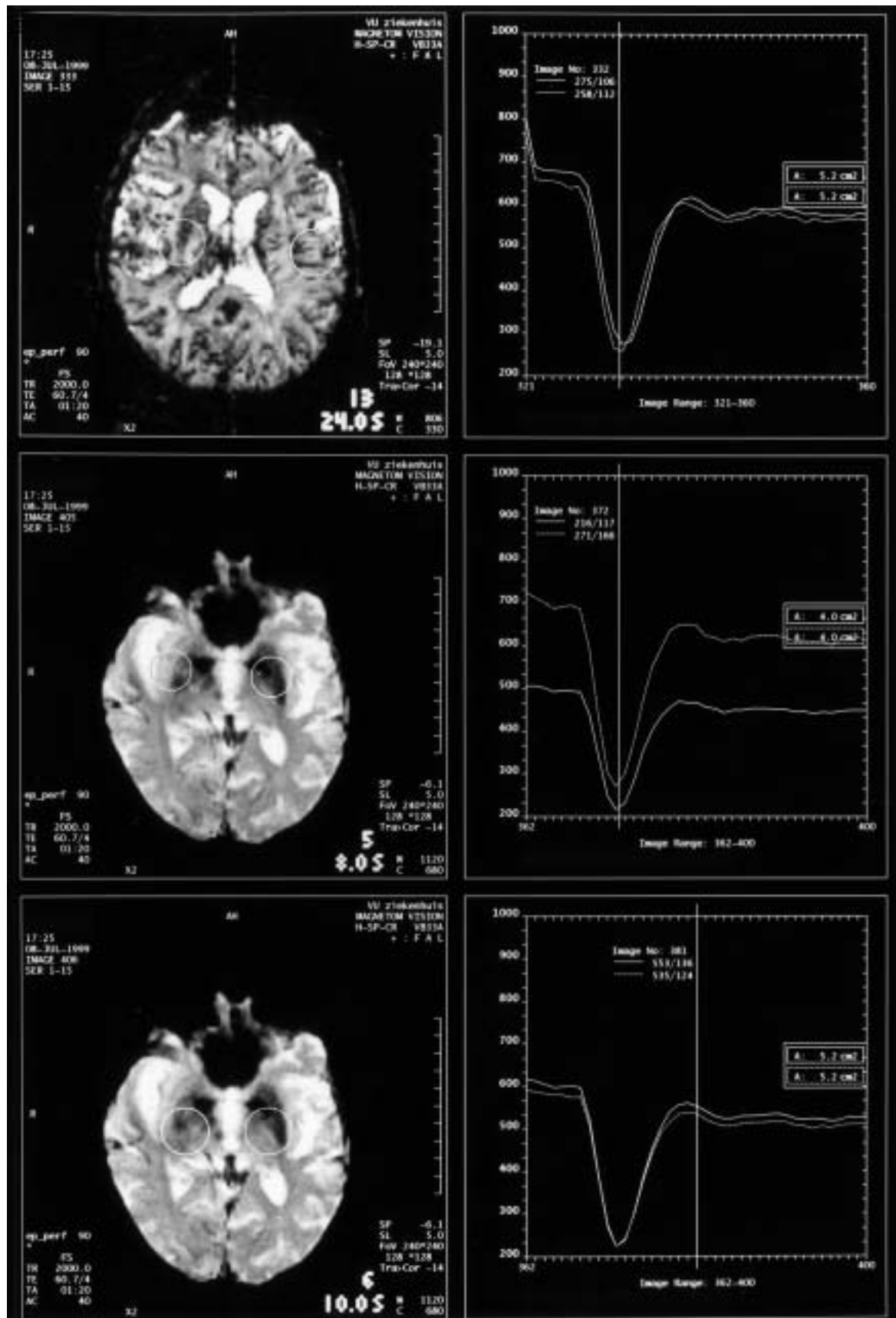
MR spectroscopy (MRS) offers the possibility of measuring in vivo the concentration of a number of brain metabolites. This can be achieved by exploiting the minor differences in resonance frequency of these metabolites, caused by the different electromagnetic environment of (for example) protons in

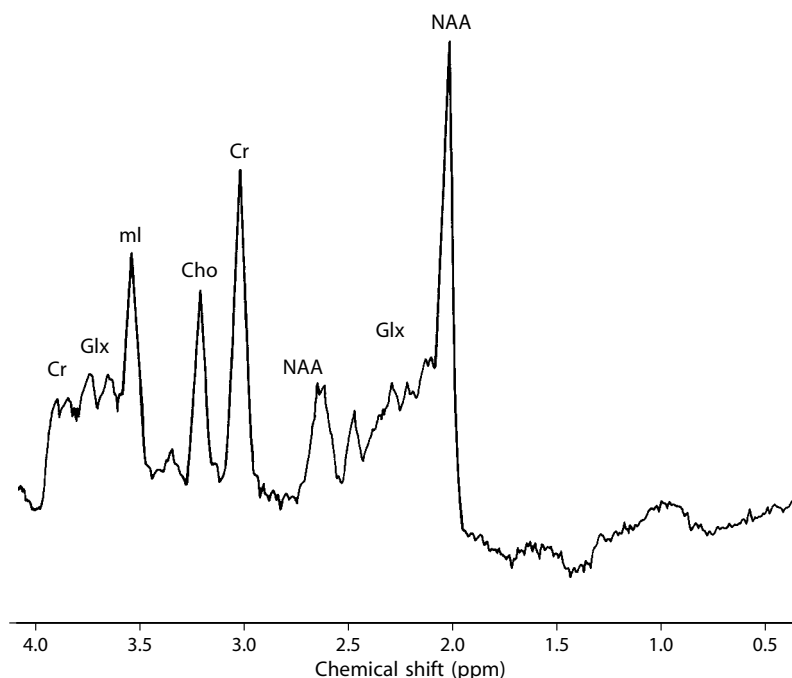
different molecules. Because of its relative simplicity, proton spectroscopy is most generally used, but MRS of other nuclei, such as phosphor or fluor, is also possible. The number of peaks seen on MRS depends on the pulse sequence used. A SE MRS sequence with long echo times will show only a few peaks: *N*-acetylaspartate (NAA), choline and creatine (and lactate when present). In so-called stimulated echo mode sequences (STEAM), allowing much shorter echo times, metabolites with a relatively short T2 relaxation time will also be detected, for example myo-inositol, scyllo-inositol and the glutamine-glutamate complex. Lactate, however, with a long T2 relaxation time, is less well seen. Studies can be performed as single voxel study with a volume of 1×1×1 cm³ or larger, or as chemical shift imaging measuring a number of voxels at the same time. In the latter technique information is obtained over a whole slice, subdivided into voxels. The overview over a larger area is sometimes helpful; the spectra, however, are usually much less resolved and shorter echo times are not easily achieved.

In MRI, the signal intensity of a voxel is determined by the amount of protons available in tissue water and tissue fat and their relaxation state. The signal of water is immense compared with that of the other proton-containing brain metabolites. To appreciate these millimolar concentrations, the water signal has to be suppressed. Water suppression can be achieved in many different ways, for example by a saturation pulse with the exact frequency of water. Once the water peak is no longer a disturbing factor, the peaks of the metabolites can be seen. Most of the peaks on MRS represent a specific aspect of the condition of the measured tissue and of the metabolic process underlying it. The metabolites usually seen on proton MRS are given in Table 2.1-1.

Table 2.1-1. Metabolites usually seen on magnetic resonance spectroscopy

Metabolite	Chemical shift (ppm)	Representing
<i>N</i> -acetylaspartate (NAA)	2.02 (2.48, 2.60)	Neurons, axons
Creatine (Cr)	3.02, 3.94	Energy level, cellular density
Choline (Cho)	3.22	Membrane turnover, neurotransmission
Myo-inositol (m-Ino)	3.56	Gliosis, osmotic balance
Glutamine, glutamate (Glu)	2.1, 2.5, 3.8	Excitatory amino acids
Lactate (Lact)	1.33 (doublet)	Anerobic glycolysis





◀ **Fig. 2.1-8.** Perfusion imaging at three levels of the brain in a 70-year-old-patient with Parkinson's disease and dementia. The *top row* compares left and right peri-insular regions. Voxels of the same size and in the same region show nearly identical perfusion patterns. In the *middle row* the region of interest (ROI, *circle*) lies somewhat more to the side. The averaged signal intensity of this area is higher and, probably because some opercular vessels are included, the perfusion curve reaches deeper (the surface under the curve reflects the relative cerebral blood volume, rCBV, of the ROI). The *bottom row* shows that when the positions left and right are similar the perfusion curves look alike again. Perfusion imaging with bolus injection has many pitfalls. Analysis can best be performed on a voxel basis, but not all vendors provide this facility for their equipment. Off line work stations and software programs are often necessary

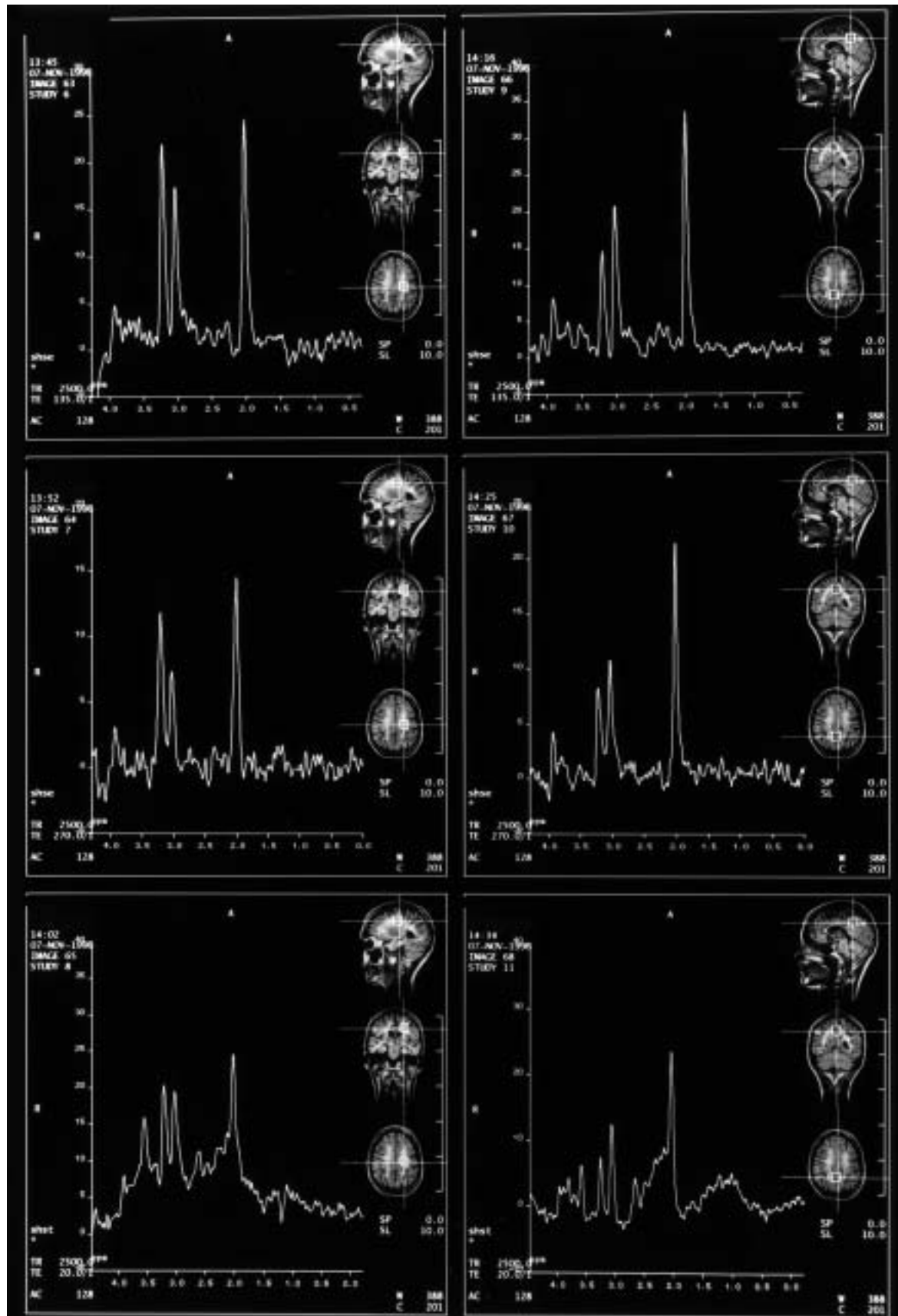
Fig. 2.1-9. Spectrum of normal volunteer made with the stimulated echo mode (STEAM) and short echo time (20 ms). NAA *N*-acetylaspartate; Glx glutamine-glutamate complex; at 2.6 ppm the second NAA peak; *Cr* creatine-containing compounds; *Cho* choline; *ml* myo-inositol; at about 3.7 ppm the second glutamate complex peaks, at 3.8 ppm the second creatine peak. At longer echo times compounds with a short T2 relaxation time are not visible in the spectrum

Within reasonable limits, it is now possible to quantify the proton MR spectra, facilitating comparison of findings in different disease states, or within patients over time. The results obtained by MRS can be divided into two categories: specific abnormalities indicating a unique disease condition and changes in the ratios of the metabolites. Specific abnormalities are mostly seen in metabolic disorders, such as phenylketonuria, hypo- or acreatinemia, excess of NAA in Canavan's disease, and of glycine in hyperglycinemia. In patients with neurodegenerative disorders the usual finding is a change in the ratio between metabolites or a general decrease in metabolites. In Alzheimer's disease a decrease in NAA is found together with an increase in myo-inositol. In frontotemporal dementia one may find the same changes, but in a different location. In vascu-

lar dementias some lactate may be present; in mitochondrial disorders the lactate is as a rule much more prominent. Loss of NAA in the basal ganglia may differentiate multisystem atrophy (MSA) from idiopathic parkinsonism. In many diseases of the central nervous system (CNS) MRS now has a place and an increasing number of centers use MRS as a source of extra information (Figs. 2.1-9, 2.1-10).

2.1.1.8 MR Neurofunctional imaging (fMRI)

The morphological information provided by MR is unique and has changed many of the insights that were commonly accepted in the neurological sciences. In the last decade, and with explosive growth in the last 5 years, MR has been used to ex-



tract functional information from the CNS. fMRI appears to have similar abilities to PET in displaying CNS responses to a variety of stimuli. The first experiments used simple paradigms. Movement of the fingers showed activation in the motor area and eventually the supplementary motor area where it could be expected. Silent speech provoked activation of the center of Broca.

fMRI uses the difference in magnetic susceptibility between oxygenated and deoxygenated blood as an intrinsic contrast medium. Deoxygenated blood has a paramagnetic effect and locally distorts the magnetic field lines, leading to dephasing and local loss of signal. Oxygenated blood has no paramagnetic effect. Influx of oxygenated blood into activated brain areas leads to a washout of deoxygenated blood resulting in a local signal increase in the images. Currently a multitude of paradigms for brain activation exist. Some are very basic, such as stroboscopic stimulation of the visual cortex, stimulation of the motor cortex by voluntary movements (either truly executed or imagined), or silent speech generation. Other paradigms are more complicated and study neuropsychological processes, such as language development and memory functions. The latter methods, allowing separate analysis of encoding, retrieval and working memory, may become of great interest in the (differential) diagnosis of early dementia, in its follow-up, and, perhaps more important in the future, in monitoring the effect of therapeutic trials with new medication. Selective activation of the hippocampus is possible with a variety of stimuli of which memory tasks and encoding tasks are the most promising so far. It is hoped that developments in paradigms and technique of analysis (e.g., event-related brain activation) will improve the reproducibility and reliability of studies of the memory system, and pave the way to a diagnostic application of fMRI in dementia (Figs. 2.1-11, 2.1-12).

- ◀ **Fig. 2.1-10.** Series of spectra in a 25-year-old woman who presented with an acute progressive neurological syndrome, with changes in consciousness, confusion, disorientation, and spastic, atactic symptoms. The *left column* represents spectra from a voxel in the abnormal white matter; the *right column* shows spectra from the relatively normal occipital cortex. The *top row* shows spectra taken with the PRESS technique and an echo time of 135 ms, TR 2500 ms, the *middle row* shows PRESS spectra with an echo time of 270 ms, and the *bottom row* shows STEAM spectra with an echo time of 20 ms. The white matter spectra are abnormal, with a decrease in *N*-acetylaspartate and elevation of choline. At 1.3 there is a small amount of lactate. The ultimate diagnosis was Marburg form of multiple sclerosis; there was improvement after treatment with high doses of methylprednisolone

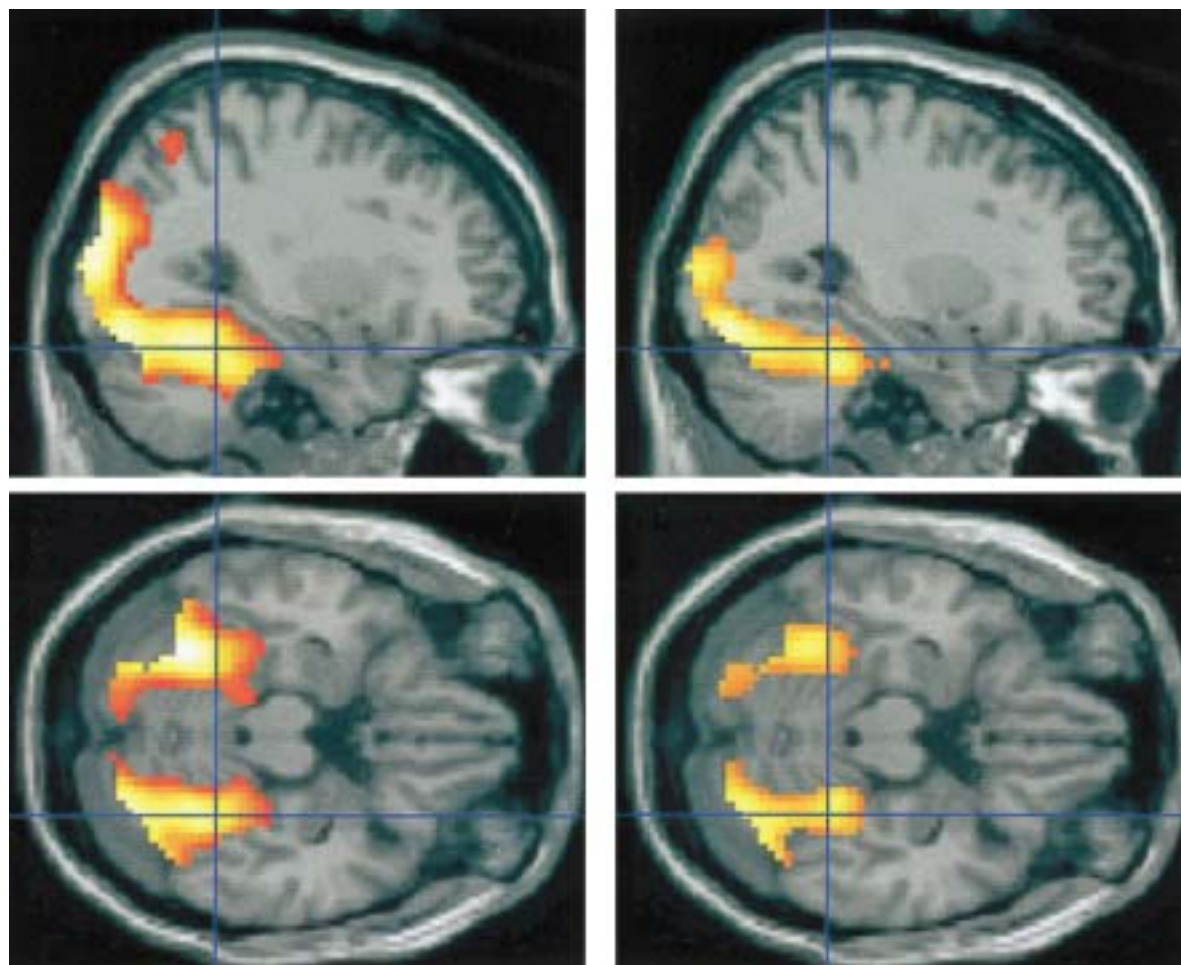
2.1.1.9 PET and SPECT in Dementia

Single photon emission computed tomography (SPECT) and positron emission tomography (PET) certainly have a role in the diagnosis and research of the dementias (Figs. 2.1-13, 2.1-14, pp. 18, 19). Perfusion studies may be very useful in establishing a diagnosis in neurodegenerative disorders. PET, because of its greater sensitivity than MR, will remain unique in the detection of abnormalities of neurotransmission, which will be of growing importance in the future.

We will illustrate the role of SPECT and PET in several chapters.

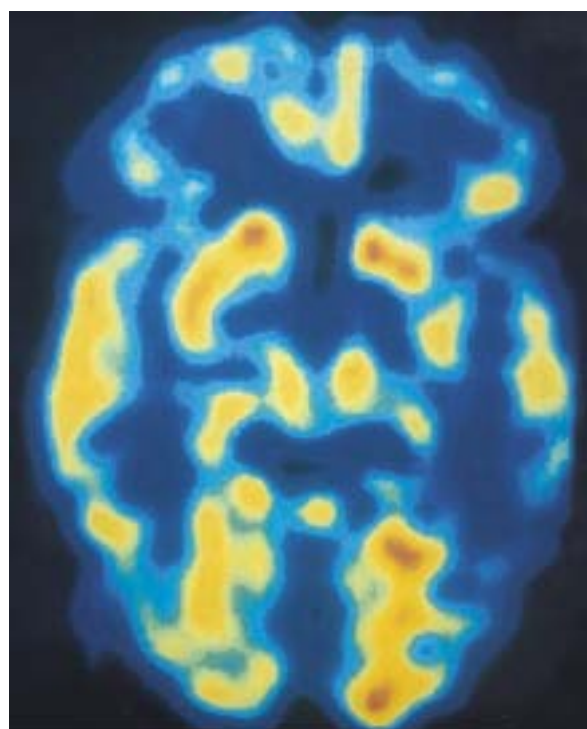


- Fig. 2.1-11.** In functional MRI activation by simple stimuli or tasks is relatively simple, when the other requirements are present. Such simple stimuli are finger, arm or leg movements to locate the motor area and visual stimuli, to locate activation in the visual cortex. In its simplest form stimuli are applied with a stroboscopic lamp with a frequency of 8 Hz and an on-off paradigm, so that the images without stimulation can be subtracted from those with activation. Postprocessing has now become much more complex and involves various kinds of statistical mapping. More complex visual stimuli look at specific patterns and at movement. In this case the brain activation after visual stimulation is superimposed on a high-resolution MR image, to determine more exactly the location of the activation



▲

Fig. 2.1-12. In continuation of the remarks with regard to Fig. 2.1-11, successful attempts have been made to selectively activate the hippocampal formation and other structures involving the memory process. This figure illustrates activation in the parahippocampal gyrus after a visual encoding task. On the *left side* a normal volunteer is shown, and on the *right side* a patient suspected of early Alzheimer's disease. Further developments of this paradigm are under way and will eventually create an instrument that will monitor the success of therapy in patients with memory disorders better than atrophy measurements on morphological MRI. (Figure kindly provided by Dr. S.A.R.B. Rombouts, VU Medical Centre, Amsterdam)



◀

Fig. 2.1-13. ^{99m}Tc -HMPAO SPECT image showing hypoperfusion in the left postero-temporal-parietal areas, more prominent on the left side. With regard to the functional analysis of neurodegenerative disorders SPECT and PET imaging and measurements are of considerable importance

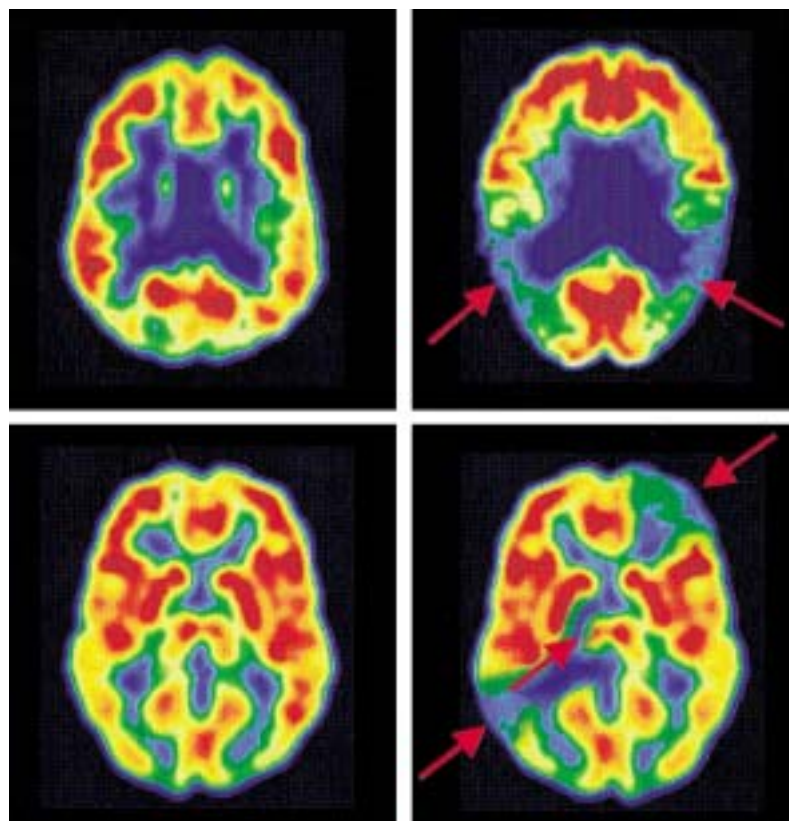


Fig. 2.1-14. PET images showing the difference between a normal age-matched control and a patient with Alzheimer's disease and multi-infarct dementia. Note the temporo-par-

ietal hypoperfusion in Alzheimer's disease and the irregular (*above*) and asymmetrical hypoperfused areas in multi-infarct dementia (*below*). (Courtesy of Gary Small, M.D.)

References and Further Reading

- Basser PJ, Pajevic S, Pierpaoli C, Duda J, Aldroubi A. In vivo tractography using DT-MRI data. *Magn Reson Med*, 2000; 44: 625-632
- Benson DF, Kuhl DE, Hawkins RA, Phelps ME, Cummings JL, Tsai SY. The fluorodeoxyglucose ^{18}F scan in Alzheimer's disease and multi-infarct dementia. *Arch Neurol*, 1983; 40: 711-714
- Bowen BC, Block RE, Sanchez-Ramos J, Pattany PM, Lampman DA, Murdoch JB, Quencer RM. Proton MR spectroscopy of the brain in 14 patients with Parkinson disease. *AJNR Am J Neuroradiol*, 1995; 16: 61-68
- Brun A, Gustafson L. Limbic lobe involvement in presenile dementia. *Arch Psychiat Nervenkr*, 1978; 226: 79-93
- Christiansen P, Schlosser A, Henriksen O. Reduced N-acetylaspartate content in the frontal part of the brain in patients with probable Alzheimer disease. *Magn Reson Imaging*, 1995; 13: 457-462
- Ernst T, Chang L, Melchor R, Mehninger CM. Frontotemporal dementia and early Alzheimer disease: differentiation with frontal lobe ^1H -MR spectroscopy. *Radiology*, 1997; 203: 829-836
- Freeborough PA, Woods RP, Fox NC. Accurate registration of serial 3D MR brain images and its application to visualizing change in neurodegenerative disorders. *J Comput Assist Tomogr* 1996; 20: 1012-1022
- Graham GD, Petroff OAC, Blamire AM, Rajkowska G, Goldman-Rakic, Prichard JW. Proton magnetic resonance spectroscopy in Creutzfeldt-Jakob disease. *Neurology*, 1993; 43: 2065-2068
- Hayman LA, Hurley RA, Puryear LJ. Pathways for declarative memory and emotion. *Int J Neuroradiol*, 1995; 1: 87-89
- Jagust WJ, Budinger TF, Reed BR. The diagnosis of dementia with single photon emission computed tomography. *Arch Neurol*, 1987; 44: 258-262
- Kaufer DI, Miller BL, Itti L, Fairbanks LA, Li J, Fishman J, Kushi J, Cummings JL. Midline cerebral morphometry distinguishes frontotemporal dementia and Alzheimer's disease. *Neurology*, 1997; 48: 978-985
- Ketonen LM. Neuroimaging of the aging brain. *Neurol Clin North Am*, 1998; 16: 581-598
- MacKay S, Ezekiel F, Sclafani de V, Meyerhoff DJ, Gerson J, Norman D, Fein G, Weiner MW. Alzheimer disease and subcortical ischemic vascular dementia: evaluation by combining MR imaging segmentation and H-1 MR spectroscopic imaging. *Radiology*, 1996; 198: 537-545
- Meguro K, Yamaguchi S, Itoh M, Fujiwara T, Yamadori A. Striatal dopamine metabolism correlated with frontotemporal glucose utilization in Alzheimer's disease: a double-tracer PET study. *Neurology*, 1997; 49: 941-945
- Meyerhoff DJ, MacKay S, Constans JM, Norman D, van Dyke C, Fein G, Weiner M. Axonal injury and membrane alterations in Alzheimer's disease suggested by in vivo

- proton magnetic resonance spectroscopic imaging. *Ann Neurol*, 1994; 36: 40–47
- Mori S, Crain BJ, Chacko VP, van Zijl PCM. Three-dimensional tracking of axonal projections in the brain by magnetic resonance imaging. *Ann Neurol* 1999; 45: 265–269
- Petroff OAC, Graham GD, Blamire AM, Al-Rayess M, Rothman DL, Fayad PB, Brass LM, Shulman RG, Prichard JW. Spectroscopic imaging of stroke in humans: histopathology correlates of spectral changes. *Neurology*, 1992; 42: 1349–1354
- Resnick SM, Costa PT. Comments on use of H-1 MR spectroscopy for diagnosis of probable Alzheimer disease. *Radiology*, 1995; 195: 14–15
- Ross BD. Biochemical considerations in ¹H spectroscopy. Glutamate and glutamine; myo-inositol and related metabolites. *NMR Biomed*, 1991; 4: 59–63
- Ross BM, Moszczynska A, Erlich J, Kish SJ. Phospholipid-metabolizing enzymes in Alzheimer's disease: increased lysophospholipid acyltransferase activity and decreased phospholipase A2 activity. *J Neurochem*, 1998; 70: 786–793
- Shank TK, Moats RA, Gifford P, Michaelis T, Mandigo JC, Izumi J, Ross BD. Probable Alzheimer disease: diagnosis with proton MR spectroscopy. *Radiology*, 1995; 195: 65–72
- Shiino A, Matsuda M, Morikawa S, Inubushi T, Akiguchi I, Handa J. Proton magnetic resonance spectroscopy with dementia. *Surg Neurol*, 1993; 39: 143–147
- Talbot PR, Lloyd JJ, Snowden JS, Neary D, Testa HJ. Choice of reference region in the quantification of single-photon emission tomography in primary degenerative dementia. *Eur J Nucl Med*, 1995; 21: 503–508
- Talbot PR, Snowden JS, Lloyd JJ, Neary D, Testa HJ. The contribution of single photon emission tomography to the clinical differentiation of degenerative cortical brain disorders. *J Neurol*, 1995; 242: 579–586
- Tedeschi G, Litvan I, Bonavita S, Bertolino A, Lundbom N, Patronas NJ, Hallett M. Proton magnetic resonance spectroscopic imaging in progressive supranuclear palsy, Parkinson's disease and corticobasal degeneration. *Brain*, 1997; 120: 1541–1552

2.2 Image Processing Techniques

(Figs. 2.2-1 to 2.2-4)

Historically, image evaluation has been performed visually, relying on the expert's personal standard of reference. This included comparison of a given examination with previous examinations performed with the same technique in other patients and controls. Only rarely were such interpretations supported by formal measurements. Examples include ventricular width or indices, typically measured with a ruler from hardcopies such as transparent films. Obviously, this type of measurements is not reliable, since the size of the structure is relatively small, and has to be compared with a calliper printed on the same film.

In the era of CT and MR, data are acquired in a digital format, which broadens the horizon for measurements. Planimetric analysis can now be performed using the scanner console or a workstation. More reliable measurements are possible without the need for calibration since the pixel size is intrinsically determined. Planimetric digital analysis enables not only diameters to be measured, but also surfaces and signal intensities (SI) of regions of interest (ROIs). ROI analysis can be expanded to provide volumetric data by multiplying the summed areas of a particular structure with the interslice distance (slice thickness plus interslice gap) according to Cavalieri's principle, to assess the volume of a given structure (valid when at least 5 slices perpendicular to the longest axis are available).

2.2.1 ROI-Based Analyses of Regional Patterns of Atrophy

Many brain structures have been examined using planimetry. Whole brain volumes have been compared between groups of patients, showing that the brains of patients with Alzheimer's disease are significantly smaller than those of healthy controls. More specifically, atrophy of the medial temporal lobe occurs, even in patients in the earliest phase of the disease. In patients with mild cognitive impairment (MCI), the volume of the medial temporal lobe (MTL) is predictive of the development of Alzheimer's disease. Other structures investigated include the entorhinal cortex, the anterior temporal pole and the corpus callosum. The last is significantly atrophied in Alzheimer's disease, irrespective of concomitant white matter changes (Hampel et al. 2000). Most of these ROI-based techniques are quite operator-dependent. Furthermore, the criteria for ROI definition vary from center to center, making it hard to compare data from different studies.

For obvious reasons, the most frequently studied structure is the hippocampal formation. Using the criteria of Jack (1994), this measurement includes Ammon's horn, subiculum, dentate gyrus, and part of the alveus. The placement of the ROIs is illustrated in Fig. 2.2-1. In normal controls, the volume of the right hippocampus is usually slightly larger than on the left side, and some authors report that females have a larger hippocampus than males. In young healthy controls, the hippocampal volume measures around 5 cm³. With normal aging, the rate of hippocampal volume loss equals 1.6% per year. This rate is significantly greater among patients with Alzheimer's disease, and amounts to almost

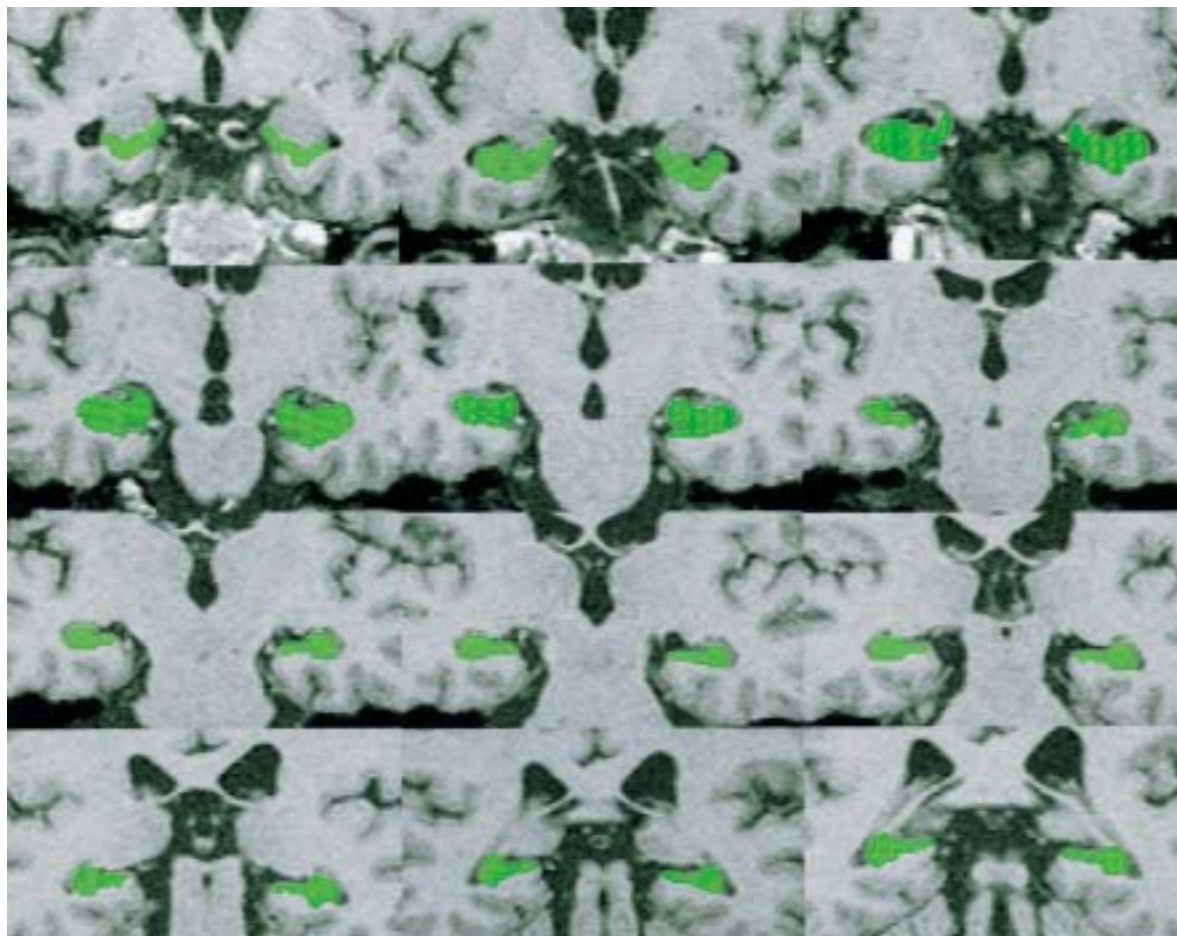


Fig. 2.2-1. A selection of coronal T1-weighted images from a 3D dataset is shown. The hippocampal formation (including Ammon's horn (CA), subiculum, dentate gyrus and part of the alveus) are indicated by green regions of interest

4% per year, an increase of approximately 2.5 times compared with age- and gender-matched control subjects (Jack et al. 1998). Convit et al. (2000) developed a method to measure other temporal lobe structures, and showed that the sensitivity and predictive value of ROI-based analyses of the temporal lobe structures (and fusiform gyrus) shift as the disease evolves. In contrast to Alzheimer's disease, in patients with dementia with Lewy bodies the hippocampus does not atrophy (Barber et al. 2000).

One of the earliest structures believed to be involved in Alzheimer's disease is the entorhinal cortex (EC). This small structure located at the antero-medial surface of the parahippocampal gyrus can be measured from high-resolution images using ROI analysis. Insausti et al. (1998) developed morphological criteria which incorporate the variable anatomical boundaries across subjects. Although atrophy of the EC is highly sensitive for Alzheimer's disease, atrophy of the EC is also found in fronto-temporal dementia (FTD), and there is considerable

interobserver variability in measuring this tiny structure (Laakso et al. 2000).

2.2.2 High-Resolution (3D) MR Imaging Techniques

The advent of high-resolution MR imaging techniques has paved the way for more advanced image postprocessing techniques. High-resolution 2D datasets and 3D datasets can now be obtained in reasonable scan times with a 1 mm isotropic spatial resolution. Examples of 3D sequences with great anatomical detail include 3D gradient echo techniques, with or without a magnetization preparation, with imaging times between 5 and 10 min. The resulting dataset is too large to be printed on film and should be viewed dynamically on a workstation for proper evaluation. ROI-based volumetric data analysis can become extremely time consuming, and is certainly not feasible for routine investigations.



Fig. 2.2-2. Voxel-based-morphometry (VBM) is a technique that compares pixel values of groups of patients after transformation to standard space. In *red*, pixels are shown with significantly lower gray-matter values in Alzheimer patients compared with controls, indicating selective gray-matter

loss in these regions. Note that besides atrophy of the hippocampus, atrophy also occurs in the caudate nucleus, in the insula and in neighboring parts of the inferior temporal gyrus. (Figure kindly provided by Dr. S.A.R.B. Rombouts, VU Medical Centre, Amsterdam)

More importantly, in many circumstances, ROI-based analysis has finite potential, since only a limited number of ROIs can be placed, the definition of which is based on a priori hypotheses. Further, as indicated above, the usefulness of a given ROI analysis may vary according to the stage of the disease, and the diagnostic setting. In clinical practice two types of questions are important. First, one would like to know where and to what extent a given examination differs from matched normal controls, in order to search for a pattern of abnormality that may lead to the diagnosis. Second, once the diagnosis is established, and repeat scanning is performed, one would like to know the changes over time.

To circumvent the limitations of ROI-based analyses as discussed above, voxel-by-voxel analysis is warranted. For the between-subjects type of analysis, i.e., cross-sectional comparison of data, voxel-based morphometry (VBM) has been developed. For within-subjects comparisons, i.e., longitudinal comparison of data within one subject over time, registration plus subtraction techniques are now available; both types of techniques will now be discussed in more detail.

2.2.3 Voxel-Based Morphometry (VBM)

The essential idea underlying VBM is a systematic comparison of pixel values between subjects, based on the assumption that the distribution of pixel values represents a biological meaningful correlate, e.g., parenchymal density. To achieve this goal, data are first registered and transferred to a standard stereotactic space, and the overall signal intensity normalized. The pixel values for each anatomical location can then be compared between groups (with correction for the large amount of statistical comparisons). VBM analysis can be performed using freely available software packages, such as Statistical Parametric Mapping (SPM). Originally developed for the analysis of functional imaging data, typically in the temporal domain, this package is well suited to comparing structural data between subjects.

VBM has been successfully applied to detect hitherto unknown abnormalities in patients with migraine, dyslexia, depression, schizophrenia and dementia. In patients with semantic dementia, a loss of tissue in the anterior pole of the temporal lobe was detected using VBM. In Alzheimer's disease, Rombouts et al. (2000) used VBM to detect symmetrical loss of tissue in the insula and caudate nuclei

(in addition to the expected atrophy in the medial temporal lobe), areas known to be affected histopathologically (Fig. 2.2-2).

For the comparison of longitudinal data (within subjects), VBM may be less well suited. During the process of transformation of data into standard stereotactic space, the data are interpolated and smoothed, perhaps leading to reduced sensitivity to change. Also, the registration method used by VBM is suboptimal. For these reasons, targeted strategies have been developed to specifically address changes over time (Freeborough et al. 1996), the general principles of which will be discussed now.

2.2.4 Registration Plus Subtraction

In the analysis of serial data, one tries to detect differences between sequential images of a subject over time. Without the use of perfect repositioning and dynamic display, small differences are extremely difficult to detect with the naked eye. Image registration is the process of matching two volumes, using algorithms such as the Wood's algorithm or Normalized Mutual Information. To avoid bias in the matching procedure by extracranial tissue, the intracranial compartment can first be extracted. Following signal normalization and rigid body matching, the volumes are subtracted. The resulting difference image can be overlaid in color to display the changes visually (Fig. 2.2-4), while the actual difference in volume can be calculated as the integral of the shift in the boundaries (as determined by SI thresholds).

Fox et al. (1996) developed a method for accurate positional matching of MRI images (registration) to enable direct comparison of volume changes of the entire brain or regions. Following 28 patients at risk for Alzheimer's disease and 26 controls for 2–3 years they found atrophy rates of 1.5% per year in the at-risk patients and 0.2% per year in the control individuals. The at-risk individuals who did not develop Alzheimer's disease had an atrophy rate of 0.1% per year. In another paper (Fox et al. 1999) they compared atrophy rates of 29 Alzheimer's disease patients and 15 controls who had had two MRI examinations with a mean interval between scans of 1.8 years. The Alzheimer's disease patients lost $2.4 \pm 1.4\%$ brain volume compared with $0.4 \pm 0.7\%$ in the controls. The correlation between loss of cognition, as measured by the Mini-Mental State Examination, and loss of brain volume was 0.80. Wahlund et al. (1999) reported that having one or two apolipoprotein-E alleles influenced the rate of atrophy in

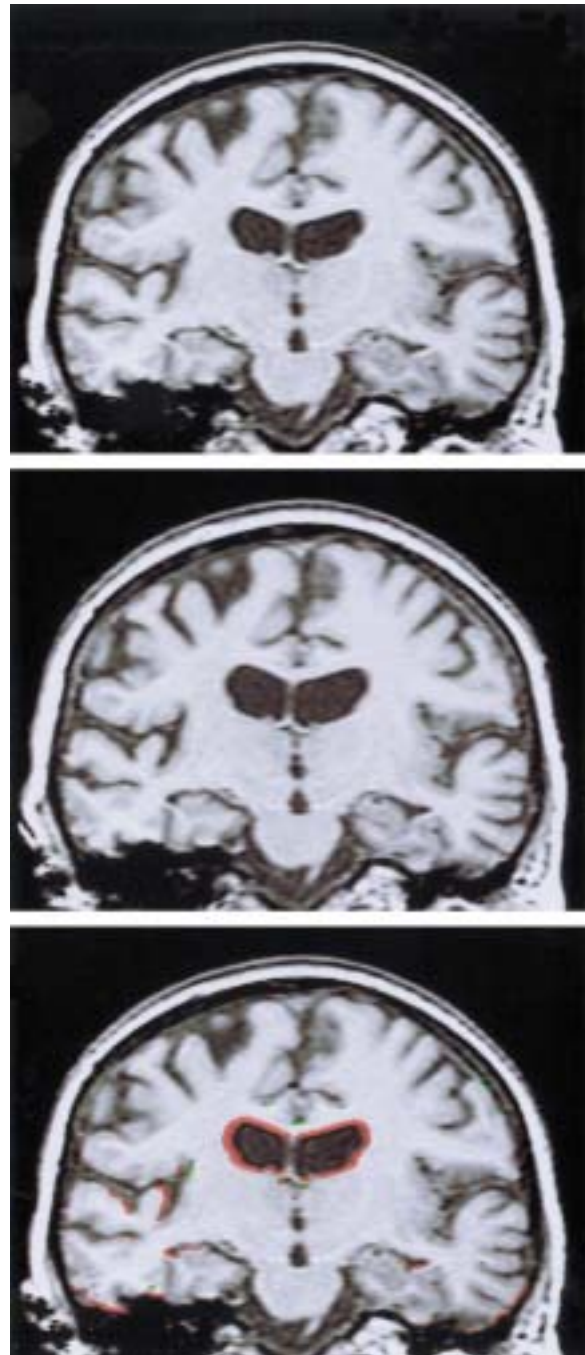


Fig. 2.2-3. Registration of scans taken at an interval of 1 year apart in a 55-year-old woman with familial risk of Alzheimer's disease. Notice the perfect alignment of the scans made at year 1 (*top panel*) and year 2 (*middle panel*) after registration. Simple visual inspection may fail to identify the progression of atrophy as shown in red (*bottom panel*) using image subtraction. (Figure kindly provided by Dr. N.C. Fox, Dementia Research Group, London)

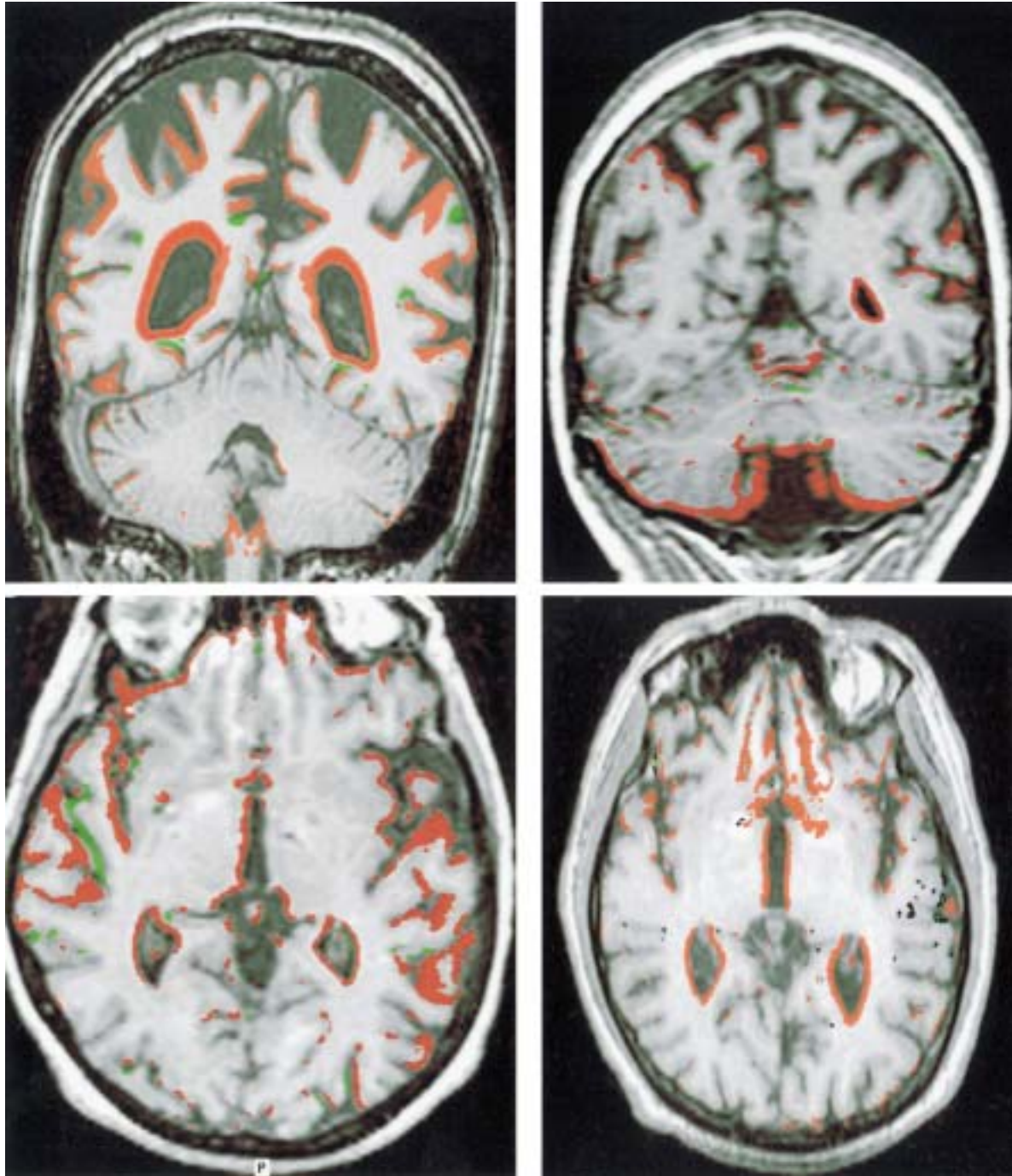


Fig. 2.2-4. Subtraction of time series can be performed after accurate image registration to show subtle changes over time that can be difficult to appreciate by visual inspection. Shown are coronal images from T1-weighted 3D data sets

obtained at yearly intervals. Note that the images are well registered with each other but that the differences (*shown in red*) are much better appreciated after subtraction. (Figure kindly provided by Dr. N.C. Fox, Dementia Research Group, London)

a set of demented and MCI patients, over a period of 16 months, using different MRI comparison techniques, but statistical significance was reached only in the non-Alzheimer's disease group.

References and Further Reading

- Barber R, Ballard C, McKeith IG, Gholkar A, O'Brien JT. MRI volumetric study of dementia with Lewy bodies: a comparison with AD and vascular dementia. *Neurology* 2000; 54: 1304–1309
- Convit A, de Asis J, de Leon MJ, Tarshish CY, De Santi S, Rusinek H. Atrophy of the medial occipitotemporal, inferior, and middle temporal gyri in non-demented elderly predict decline to Alzheimer's disease. *Neurobiol Aging*, 2000; 21: 19–26
- Ebmeier KP, Glabus MF, Prentice N, Ryman A, Goodwin GM. A voxel-based analysis of cerebral perfusion in dementia and depression of old age. *Neuroimage*, 1998; 7: 199–208
- Fox NC, Freeborough PA, Rossor MN. Visualisation and quantification of rates of atrophy in Alzheimer's disease. *Lancet*, 1996; 348: 94–97
- Fox NC, Scahill RI, Crum WR, Rossor MN. Correlation between rates of brain atrophy and cognitive decline in AD. *Neurology*, 1999; 52: 1687–1689
- Freeborough PA, Woods RP, Fox NC. Accurate registration of serial 3D MR brain images and its application to visualizing change in neurodegenerative disorders. *J Comput Assist Tomogr*, 1996; 20: 1012–1022
- Hampel H, Teipel SJ, Alexander GE, Horwitz B, Pietrini P, Hippus H, Moller HJ, Schapiro MB, Rapoport SI. Corpus callosum measurement as an in vivo indicator for neocortical neuronal integrity, but not white matter pathology, in Alzheimer's disease. *Ann N Y Acad Sci*, 2000; 903: 470–476
- Insausti R, Juottonen K, Soininen H, Insausti AM, Portanen K, Vainio P, Laakso P, Pitkanen A. MR volumetric analysis of the human entorhinal, perirhinal and temporopolar cortices. *AJNR Am J Neuroradiol*, 1998; 19: 659–671
- Jack CR. MRI-based hippocampal volume measurements in epilepsy. *Epilepsia*, 1994; 35 [Suppl 6]: S21–29
- Jack CR, Petersen RC, Xu Y, O'Brien PC, Smith GE, Ivnik RJ, Tangalos EG, Kokmen E. Rate of medial temporal lobe atrophy in typical aging and Alzheimer's disease. *Neurology*, 1998; 51: 993–999
- Kaufer DI, Miller BL, Itti L, Fairbanks LA, Li J, Fishman J, Kushi J, Cummings JL. Midline cerebral morphometry distinguishes frontotemporal dementia and Alzheimer's disease. *Neurology*, 1997; 48: 978–985
- Laakso MP, Frisoni GB, Kononen M, Mikkonen M, Beltramello A, Geroldi C, Bianchetti A, Trabucchi M, Soininen H, Aronen HJ. Hippocampus and entorhinal cortex in frontotemporal dementia and Alzheimer's disease: a morphometric MRI study. *Biol Psychiatry*, 2000; 47: 1056–1063
- Rombouts SA, Barkhof F, Witter MP, Scheltens P. Unbiased whole-brain analysis of gray matter loss in Alzheimer's disease. *Neurosci Lett*, 2000; 285: 231–233
- Wahlund LO, Julin P, Lannfelt L, Lindqvist J, Svensson L. Inheritance of the ApoE epsilon4 allele increases the rate of brain atrophy in dementia patients. *Dement Geriatr Cogn Disord* 1999; 10: 262–268
- Webb J, Guimond A, Eldridge P, Chadwick D, Meunier J, Thirion J-Ph, Roberts N. Automatic detection of hippocampal atrophy on magnetic resonance images. *Magn Reson Imaging*, 1999; 8: 1149–1161

<http://www.springer.com/978-3-540-41731-6>

Magnetic Resonance in Dementia

Barkhof, F.; Valk, J.; Fox, N.C.; Scheltens, P.

2002, X, 353 p., Hardcover

ISBN: 978-3-540-41731-6